# Fabry-Perot Interferometry with Fractional Charges

D. T. McClure, W. Chang, C. M. Marcus, L. N. Pfeiffer, and K. W. West

Phys. Rev. Lett. **108**, 256804 — Published 19 June 2012

DOI: 10.1103/PhysRevLett.108.256804

# Fabry-Perot Interferometry with Fractional Charges

D. T. McClure,[1] W. Chang,[1] C. M. Marcus,[1] L. N. Pfeiffer,[2] and K. W. West[2]

[1]*Department of Physics, Harvard University, Cambridge, Massachusetts 02138, USA*
[2]*Department of Electrical Engineering, Princeton University, Princeton, New Jersey 08544, USA*

Resistance oscillations in electronic Fabry-Perot interferometers near fractional quantum Hall (FQH) filling factors $1/3, 2/3, 4/3$ and $5/3$ in the constrictions are compared to those near integer quantum Hall (IQH) filling factors in the same devices and at the same gate voltages. Two-dimensional plots of resistance versus gate voltage and magnetic field indicate that all oscillations are Coulomb dominated. A charging-model analysis of gate-voltage periods yields an effective tunneling charge $e^* \approx e/3$ for all FQH states and $e^* \approx e$ for IQH states. Temperature decay of the oscillations appears exponential, qualitatively consistent with a recent prediction, and the surprising filling-factor dependence of the associated energy scale may shed light on edge structure.

Like their optical analogs, electronic Fabry-Perot interferometers allow quantum interference to be probed via tunable parameters that induce periodic transmission oscillations. Moreover, working with charged excitations in quantum Hall edge states, these devices feature an interplay of coherence, interaction, and magnetic effects; notably, such devices could demonstrate anyonic [1] and non-Abelian [2–5] statistics and potentially comprise topologically protected qubits [6]. In the integer quantum Hall (IQH) regime, recent experimental [7–10] and theoretical [11, 12] work has extended the results of initial experiments [13–17] and clarified the role of Coulomb interactions. Behavior consistent with Aharonov-Bohm (AB) interference of non-interacting electrons was recently observed [9, 10], and can be qualitatively distinguished from the Coulomb-dominated (CD) type using a 2D plot of resistance versus magnetic field and gate voltage.

In the fractional quantum Hall (FQH) regime, signatures of fractional charge [11] and both Abelian [1, 12] and non-Abelian [2, 5] statistics have been predicted in both the CD [2, 5, 11, 12] and AB [1, 2, 5, 12] regimes, but few experimental results have been published. Resistance oscillations generally occur when the interferometer resistance deviates slightly from a plateau, indicating weak tunneling through an IQH or FQH state in the constrictions; we will classify oscillations according to $f_c$, this state's rational filling factor. Camino et al. [18] first observed oscillations at $f_c = 1/3$ consistent with CD-regime tunneling of charge-$e/3$ quasi-particles, though other explanations may be possible [9, 18]; Ofek et al. [10] later reported a similar result that included a 2D plot justifying a CD-regime explanation. Weaker oscillations have been reported [19] near $f_c = 7/3$ and $5/2$, though apparent device instability hampers their interpretation. This experiment [19], shot-noise measurements near FQH states in the first [20, 21] and second [22] Landau levels, and related theoretical work [23, 24] suggest the possibility of tunneling mediated by quasi-particles with a larger charge than expected. Analysis of CD oscillations can reveal the charge of tunneling quasi-particles, but such measurements have not been reported for $f_c$ other than $1/3$, where experiments have consistently found the expected charge.

In this Letter, we report measurements of CD oscillations near the low-magnetic-field edges of quantized plateaus associated with several IQH and FQH states: $f_c = r = 1, 2, 3, 4$ and $f_c = r/3 = 1/3, 2/3, 4/3, 5/3$. The dependence of gate-voltage periods on $f_c$ is well described by a charging model [11, 12], allowing extraction of effective charges consistent with $e^* \approx e/3$ for fractional $f_c$ and $e^* \approx e$ for integer $f_c$. Magnetic-field periods are roughly proportional to $1/r$ in both the integer and fractional regimes, also consistent with the model. The oscillation amplitudes decay exponentially with temperature, as anticipated theoretically [12], but with a surprising pattern: the associated temperature scale is different for the IQH and FQH regime, but otherwise independent of $f_c$ and device area.

Interferometers were fabricated using e-beam lithography on GaAs/AlGaAs heterostructures with a two-dimensional electron gas (2DEG) of density $n_b = 1.7 \times 10^{11}$ cm$^{-2}$ and mobility $\mu = 2 \times 10^7$ cm$^2$/Vs in a 40-nm quantum well centered 290 nm below the surface. A $BCl_3$ reactive ion etch formed 150 nm deep trenches [25] into which Ti/Au gates were deposited in the same litho-

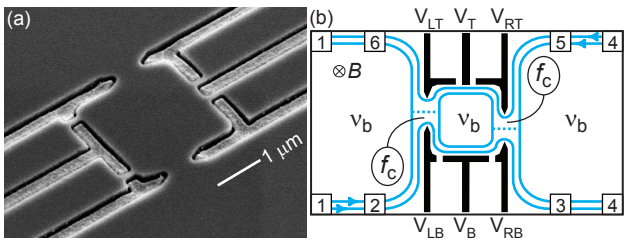


FIG. 1. (a) Scanning electron micrograph of a typical interferometer. (b) Gate layout of the 4 $\mu$m$^2$ device with schematic diagram of edge state paths, filling factors, and ohmic contacts. A current bias applied between contacts 1 and 4 allows measurement of diagonal resistance $R_D$ (contacts $2-5$) and Hall resistance $R_{xy}$ (contacts $3-5$). This picture assumes that only one edge is partially transmitted by the interferometer, while others are fully transmitted or reflected. For clarity, only one fully-transmitted edge and no fully-reflected edges are shown.

graphic step [Fig. 1(a)]. Measurements on two devices are reported, one with lithographic area $A_{\rm lith} = 4\ \mu{\rm m}^2$ and 750 nm constrictions [identical to the device in Fig. 1(a), and shown schematically in Fig. 1(b)] and the other with $A_{\rm lith} = 2\ \mu{\rm m}^2$, 600 nm constrictions, and a single gate $V_{\rm B}$ in place of gates $V_{\rm LB}, V_{\rm B}, V_{\rm RB}$. Devices were cooled in a dilution refrigerator with base temperature $\lesssim 10$ mK [26]. The interferometer's diagonal resistance $R_{\rm D}$ [27] and the bulk Hall resistance $R_{\rm xy}$ were measured simultaneously using LI-75A pre-amplifiers from NF Corporation followed by a lock-in with ac current bias $I = 0.25$ nA [Fig. 1(b)] and time constant $\sim 0.5$ s.

Figure 2(a) shows $R_{\rm xy}$ and $R_{\rm D}$ of the 4 $\mu{\rm m}^2$ device as a function of perpendicular magnetic field $B$, covering filling factors from 2/3 to 3 in both constrictions and bulk. Voltages of $\sim -200$ mV on gates $V_{\rm LT}, V_{\rm RT}, V_{\rm LB}$, and $V_{\rm RB}$ reduced electron density in both constrictions by $\sim 10\%$ compared to the bulk, while preserving several FQH plateaus. Oscillations in $R_{\rm D}$ (Fig. 2 insets) were observed at the low-field edges of several IQH and FQH plateaus, where presumably the only forward transmission of the interfering edge occurs via weak forward tunneling through the $f_{\rm c}$ quantum Hall state [Fig. 1(b)]. Gate-voltage adjustments allowed variation of the magnetic field (and thereby the bulk filling factor $\nu_{\rm b} = n_{\rm b}h/eB$) where each plateau and its associated oscillations appeared; as in the lower panel of the $f_{\rm c} = 2/3$ inset. Even as $\nu_{\rm b}$ was thus tuned through a range of compressible and incompressible states, the magnetic-field and gate-voltage periods at each $f_{\rm c}$ remained nearly constant. The slight period difference between the two $f_{\rm c} = 2/3$ inset panels [more apparent as a frequency difference in Fig. 3(d)] is consistent with reduced device area at more negative gate voltages. Two-dimensional sweeps of magnetic field and gate voltage [Figs. 2(b-e)] show positively sloped constant-phase lines, indicating CD oscillations [9].

Field and gate periods were extracted from fast Fourier transforms (FFT's) [Fig. 3], which all show a sharp peak at a single frequency. A gaussian fit to the peak gives the center frequency $f_0$ and full width at half-maximum $\delta f$, with periods $\Delta B$ or $\Delta V_{\rm g}$ given by $1/f_0$. For FFT's over $N_{\rm osc}$ oscillations, we find $\delta f \sim 1/N_{\rm osc}$, indicating that the uncertainty results from the finite data range.

Similar oscillations appeared in the 2 $\mu{\rm m}^2$ device, and at $f_{\rm c} = 1/3, 5/3, 3$ and 4. The remaining figures present three data sets, with the same gate voltages used at all integer and fractional $f_{\rm c}$ within each. Gate periods [Fig.. 4(a)] are normalized by their values at $f_{\rm c} = 1$, allowing comparison of periods from all four gates common to both devices. A steady increase in $\Delta V_{\rm g}$ with $f_{\rm c}$ appears in the FQH regime, with a similar but weaker trend in the IQH regime. Field periods [Fig. 4(b)] appear proportional to $1/r$, where $f_{\rm c} = r$ in the IQH regime and $f_{\rm c} = r/3$ in the FQH regime. Separate fit lines of the form $\Delta B \propto 1/r$ agree with data from each regime in each data set, with slightly larger slopes in the FQH regime than in the IQH regime.

We next summarize the theoretical charging model [11, 12] used to analyze the data [28]. In this model, oscillations can arise from charge balancing in a nearly isolated island of charge, coupled to the leads via weak forward tunneling, with charging events occurring in units of the quasi-particle charge $e^*$ in the constrictions. This charge is expected to depend not on the identity of the partitioned edge, but instead on the state $f_{\rm c}$: for integer $f_{\rm c}$, $e^* = e$, and for $f_{\rm c} = r/s$, the composite fermion model [29] predicts $e^* = e/s$. The charge on the island is $N_{\rm L}e^*$, with $N_{\rm L}$ quantized to an integer value. The 2DEG in this area also contains continuous negative charge $N_\phi f_{\rm c} e$ from the lower-energy electrons, where $N_\phi = BA/\phi_0$ is the (non-quantized) number of quanta of flux, $\phi_0 = h/e$, in the area $A$ enclosed by the interfering edge. To minimize energy, the total negative charge must balance the background positive charge $N_{\rm BG}|e|$ from ionized donors (positive) and gate voltages (negative), yielding the charge neutrality equation $N_\phi f_{\rm c} e + N_{\rm L} e^* \approx N_{\rm BG} e$, where quantization of $N_{\rm L}$ prevents exact equality. Expressing $N_\phi$ and $N_{\rm BG}$ in terms of gate voltage and magnetic field, and finding the change in these parameters needed to induce a unit change in $N_{\rm L}$, allows calculation of oscillation periods.

Gate voltages affect the charge balance in three ways: through the enclosed flux via area, with $\beta_{\rm g} \equiv dN_\phi/dV_{\rm g} = (B/\phi_0)(dA/dV_{\rm g})$, and through the background charge via both density $n_{\rm BG}$ and area. Summing the two background charge effects gives $\gamma_{\rm g} \equiv dN_{\rm BG}/dV_{\rm g} = n_{\rm BG}(dA/dV_{\rm g}) + A(dn_{\rm BG}/dV_{\rm g})$, which is assumed $B$-independent [12]. For fixed magnetic field, the charge neutrality equation then yields the gate-voltage period

$$\Delta V_{\rm g} = \frac{e^*/e}{\gamma_{\rm g} - \beta_{\rm g} f_{\rm c}}. \qquad (1)$$

This result reflects the Coulomb-blockade intuition that $\Delta V_{\rm g} \propto e^*$, but here the gating effect of the lower-energy electrons, represented by $\beta_{\rm g} f_{\rm c}$, may cause the lever-arm to depend on $f_{\rm c}$: although $\beta_{\rm g} \propto B$ and $f_{\rm c} \sim 1/B$, the second relationship is inexact since plateau widths are nonzero and $f_{\rm c}$ is discrete. Considering oscillations at the low-field edges of plateaus, those near weaker plateaus will have larger $\beta_{\rm g} f_{\rm c}$, hence larger $\Delta V_{\rm g}$, consistent with the data in Fig. 4(a). An $f_{\rm c}$-independent lever-arm would be obtained for $dA/dV_{\rm g} = 0$, i.e. for an ideal back gate, but both the geometry of our device and the observed $f_{\rm c}$-dependence of $\Delta V_{\rm g}$ suggest that the gates mainly affect the area.

Assuming ideal side gates (i.e. $dn_{\rm BG}/dV_{\rm g} = 0$) and an infinitely steep confining potential allows consolidation of $\gamma_{\rm g}$ and $\beta_{\rm g}$: $\gamma_{\rm g} - \beta_{\rm g} f_{\rm c} = \eta_{\rm g}(B_1 - B f_{\rm c})$, where $\eta_{\rm g} = \beta_{\rm g}/B$ is the only free parameter and $B_1 = n_{\rm b}\phi_0$ is the field at which $\nu_{\rm b} = 1$. Then $\eta_{\rm g}$ may be extracted from $\Delta V_{\rm g}$ measured at a single $f_{\rm c}$ with known $e^*$ (we choose

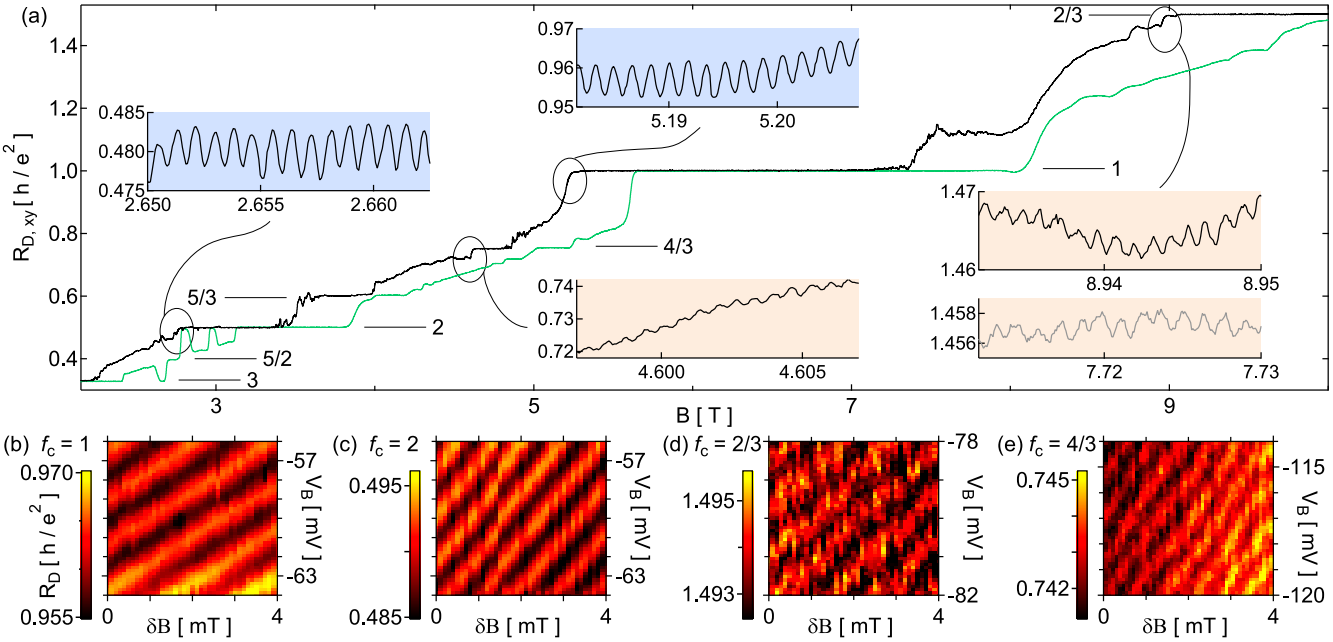


FIG. 2. (a) Resistances $R_{\rm D}$ (black) and $R_{\rm xy}$ (green) as a function of perpendicular magnetic field $B$, with $V_{\rm T}$ and $V_{\rm B}$ near $-100$ mV and all other gate voltages near $-200$ mV. Numbered horizontal lines indicate filling factors of notable quantum Hall plateaus. Insets: detail views of $R_{\rm D}$, revealing oscillations at $f_{\rm c} = 1$ (top), 2 (left), 2/3 (right), and 4/3 (bottom). For the lower panel in the $f_{\rm c} = 2/3$ inset, constriction gate voltages are near $-500$ mV. All features are independent of the field sweep rate (typically $\sim 20$ mT/min) and direction. Here and throughout, blue (orange) indicates integer (fractional) $f_{\rm c}$. (b-e) Plots of $R_{\rm D}$ in the $B - V_{\rm B}$ plane, with gate voltages comparable to those in (a); $B = B_0 + \delta B$, with $B_0 = 5.200$ T, 2.670 T, 8.831 T, and 4.684 T, respectively.

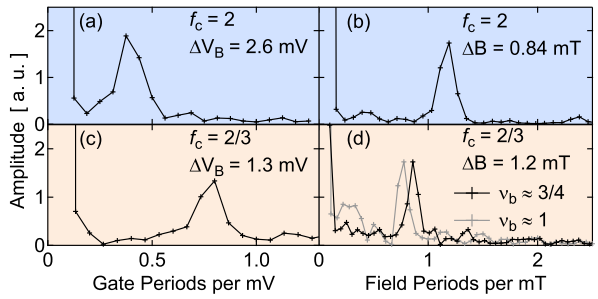


FIG. 3. Sample FFT's of oscillations with respect to $V_{\rm B}$ and $B$, for $f_{\rm c} = 2$ and 2/3. Raw data for (b) and (d) are shown in the corresponding Fig. 2(a) insets, while raw data for (a) and (c) are vertical cuts from 2D plots as in Figs. 2(c,d) but with a larger gate-voltage range for greater frequency resolution.

$f_{\rm c} = 1$), and finally used at all other $f_{\rm c}$ to calculate $e^*$ from each $\Delta V_{\rm g}$ . Performing this calculation for each gate and each data set yields the values shown in Fig. 4(c), approximately $e/s$ for all $f_{\rm c}$.

A similar analysis of the charge neutrality equation, assuming fixed gate voltages instead of fixed $B$, predicts

$$\Delta B = \frac{\phi_0}{rA}, \qquad (2)$$

where dependence on $e^*$ has been absorbed by taking $e^* = e/s$ (justified by the gate-voltage analysis), leaving $A$ as the only fit parameter. As apparent from Fig. 4(d), where Eq. 2 has been used to extract $A$ from each period in Fig. 4(b), fractional $f_{\rm c}$ consistently have slightly smaller areas than integer $f_{\rm c}$ within the same data set, similar to a previous result [18]. The area difference between the two data sets in the 2 $\mu$m$^2$ device reflects the use of less-negative gate voltages for the data set with larger areas.

To study factors that may limit oscillation amplitudes, oscillations as a function of $B$ were measured at a series of mixing chamber temperatures $T$, and the average frequencies and amplitudes of the oscillations at each $f_{\rm c}$ were extracted at each temperature. The frequencies are $T$-independent, but the amplitudes depend strongly on $T$, as shown in Fig. 5, where each data set is normalized by its value at the lowest temperature. Each data set can be characterized by an exponential decay of the form $De^{-T/T_0}$, where $T_0$ represents a characteristic temperature scale. The continuation of this behavior down to the lowest temperatures confirms that the 2DEG was well thermalized to the mixing chamber even for $T \lesssim 10$ mK; furthermore, IQH regime data up to 100 mK (not shown) remain consistent with an exponential dependence, different from the power-law behavior observed in the IQH regime at higher temperatures [30]. The $T_0$ values differ significantly between the IQH and FQH regimes but otherwise appear insensitive to both $f_{\rm c}$ and area.

Ref. [12] hints at a physical interpretation of the exponential dependence and the difference in $T_0$ between the

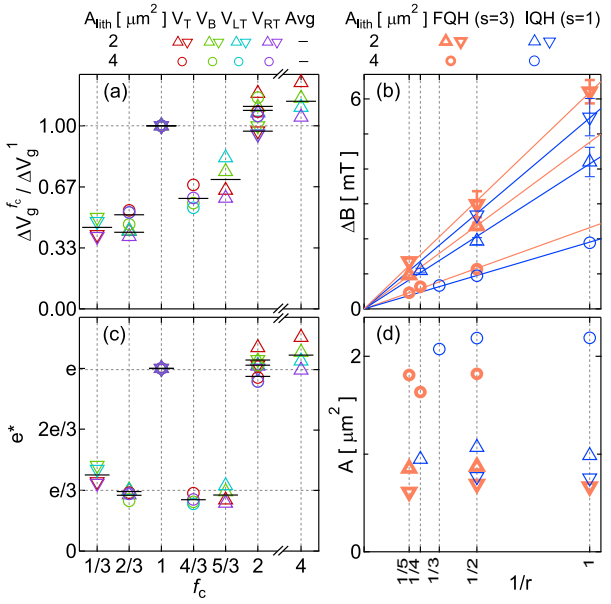


FIG. 4. (a) Gate periods $\Delta V_{\rm T}$ (red), $\Delta V_{\rm B}$ (green), $\Delta V_{\rm LT}$ (aqua) and $\Delta V_{\rm RT}$ (purple), and their average (horizontal black lines), as a function of $f_{\rm c}$, normalized by their values at $f_{\rm c} = 1$. Throughout Figs. 4 and 5, two data sets are taken from the 2 $\mu$m$^2$ device (triangles) and one from the 4 $\mu$m$^2$ device (circles). (b) Field periods of IQH ($f_{\rm c} = r$) [thin, blue] and FQH ($f_{\rm c} = r/3$) [thick, orange] oscillations versus $1/r$. Error bars, corresponding to FFT peak widths, are omitted when smaller than markers. Fit lines have slopes 1.9, 2.3, 4.1, 4.8, 5.4, and 6.2 mT from bottom to top. (c) Effective charges $e^*$ extracted from the gate periods shown in (a) using Eq. 1, assuming $e^* = e$ at $f_{\rm c} = 1$. (d) Effective areas calculated using Eq. 2 from the values of $\Delta B$ shown in (b).

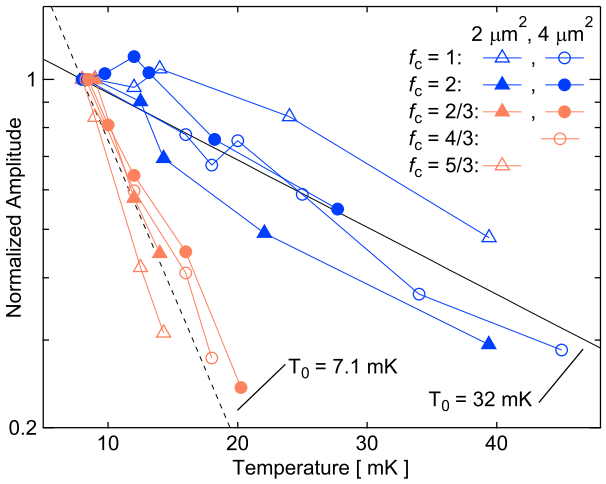


FIG. 5. Temperature dependence of oscillation amplitude at several filling factors in the IQH (blue) and FQH (orange) regimes. Lines are given by $De^{-T/T_0}$, with $T_0$ representing the average value obtained from fits to the individual data sets in each regime. Integer $f_{\rm c}$ have an average $T_0 = 32$ mK and standard deviation 7.0 mK, while fractional $f_{\rm c}$ have average $T_0 = 7.1$ mK with standard deviation 1.8 mK; in both cases, any dependence on filling factor or device size is smaller than the measurement uncertainty. Data at $f_{\rm c} = 4$ were similar to those at $f_{\rm c} = 1, 2$ and therefore omitted for clarity; data at $f_{\rm c} = 1/3$ were unobtainable because of device drift. Above 20 mK, FQH-regime oscillations were immeasurably small.

two regimes: $T_0$ is related to an effective charging energy $E_m = (e^*)^2/C_{\rm eff}$, where $C_{\rm eff}$ is determined by both the capacitance of the island and edge-structure details [31]. Using this expression with $e^* = e/s$, the measured $T_0$ yield $C_{\rm eff}$ twice as large in the IQH regime as in the FQH regime. Since $T_0$ appears insensitive to area, this difference cannot be attributed directly to the area difference between the two regimes; instead, both likely result from a more general structural difference between the IQH and FQH regimes.

In summary, analysis of gate-voltage periods reveals a quasi-particle charge close to $e/3$ at all FQH states studied, a result that agrees with previous work at $f_{\rm c} = 1/3$, adds to a complicated story at $f_{\rm c} = 2/3$, and constitutes the first published value at $f_{\rm c} = 4/3$ and $5/3$. Magnetic-field periods imply slightly different effective areas for fractional and integer $f_{\rm c}$. The temperature scales on which the oscillations decay suggest the existence of further structural differences between the two regimes.

We acknowledge useful discussions with A. Kou, B. I. Halperin, B. Rosenow, and I. Neder, and funding from Microsoft Corporation Project Q, IBM, NSF (DMR-0501796), and Harvard University. Device fabrication at Harvard Center for Nanoscale Systems.

[1] C. de C. Chamon *et al.*, Phys. Rev. B **55**, 2331 (1997).
[2] A. Stern and B. I. Halperin, Phys. Rev. Lett. **96**, 016802 (2006).
[3] P. Bonderson, A. Kitaev, and K. Shtengel, Phys. Rev. Lett. **96**, 016803 (2006).
[4] R. Ilan, E. Grosfeld, and A. Stern, Phys. Rev. Lett. **100**, 086803 (2008).
[5] A. Stern *et al.*, Phys. Rev. B **82**, 085321 (2010).
[6] C. Nayak *et al.*, Rev. Mod. Phys. **80**, 1083 (2008).
[7] M. D. Godfrey *et al.* (2007), arXiv:0708.2448.
[8] F. E. Camino, W. Zhou, and V. J. Goldman, Phys. Rev. B **76**, 155305 (2007).
[9] Y. Zhang *et al.*, Phys. Rev. B **79**, 241304 (2009).
[10] N. Ofek *et al.*, Proc. Natl. Acad. Sci. USA **107**, 5276 (2010).
[11] B. Rosenow and B. I. Halperin, Phys. Rev. Lett. **98**, 106801 (2007).
[12] B. I. Halperin *et al.*, Phys. Rev. B **83**, 155440 (2011).
[13] B. J. van Wees *et al.*, Phys. Rev. Lett. **62**, 2523 (1989).
[14] B. W. Alphenaar *et al.*, Phys. Rev. B **46**, 7236 (1992).
[15] P. L. McEuen *et al.*, Phys. Rev. B **45**, 11419 (1992).
[16] R. P. Taylor *et al.*, Phys. Rev. Lett. **69**, 1989 (1992).
[17] J. P. Bird *et al.*, Phys. Rev. B **53**, 3642 (1996).
[18] F. E. Camino, W. Zhou, and V. J. Goldman, Phys. Rev. Lett. **98**, 076805 (2007).
[19] R. L. Willett, L. N. Pfeiffer, and K. W. West, Phys. Rev. B **82**, 205301 (2010).
[20] Y. C. Chung, M. Heiblum, and V. Umansky, Phys. Rev. Lett. **91**, 216804 (2003).
[21] A. Bid *et al.*, Phys. Rev. Lett. **103**, 236802 (2009).

[22] M. Dolev *et al.*, Phys. Rev. B **81**, 161303 (2010).
[23] D. Ferraro *et al.*, Phys. Rev. B **82**, 085323 (2010).
[24] M. Carrega *et al.*, Phys. Rev. Lett. **107**, 146404 (2011).
[25] The trenches improve device performance in two ways: their steep confining potential allows the formation of sub-micron constrictions with $f_c \approx \nu_b$, and the elimination of the donor layer between the gates and the 2DEG enhances stability.
[26] Evidence that the 2DEG also reaches this temperature is presented in Fig. 5 and the associated discussion.
[27] C. W. J. Beenakker and H. van Houten, Solid State Physics **44**, 1 (1991).
[28] In the regime of our oscillations, Ref. [12]'s terminology relates to ours as follows: $\nu_{out} = f_c$ and $\nu_{in} \lesssim \nu_b$.
[29] J. K. Jain, *Composite Fermions* (Cambridge University Press, 2007).
[30] B. Hackens *et al.*, Nature Comms. **1**, 39 (2010).
[31] Specifically, Ref. [12] predicts decay as $e^{-2\pi^2 k_B T/E_m}$; comparison to our model-neutral form gives $E_m = 2\pi^2 k_B T_0$. The large prefactor may explain our ability to resolve $T_0 < eV/k_B$, where $V = R_D I$.